In situ and remote characterization of the external field temporal variations at Mars

Benoit Langlais, François Civet, Erwan Thébault

AGU PUBLICATIONS

JGR

Journal of Geophysical Research: Planets

RESEARCH ARTICLE

10.1002/2016JE005060

In situ and remote characterization of the external field temporal variations at Mars

Benoit Langlais[1], **François Civet**[1], **and Erwan Thébault**[1]

[1] Laboratoire de Planétologie et Géodynamique, CNRS UMR 6112, Université de Nantes, Nantes, France

Key Points:
- Temporal variability of the external field at Mars is characterized with in situ measurements
- Strong correlation is found with ACE measurements extrapolated from Earth's orbit to Mars
- A proxy of the temporal variability is defined to help for data selection purposes

Supporting Information:
- Figure S1
- Figure S2
- Figure S3
- Figure S4
- Text S1

Correspondence to:
B. Langlais,
benoit.langlais@univ-nantes.fr

Citation:
Langlais, B., F. Civet, and E. Thébault (2017), In situ and remote characterization of the external field temporal variations at Mars, *J. Geophys. Res. Planets*, *122*, 110–123, doi:10.1002/2016JE005060.

Received 21 APR 2016
Accepted 14 DEC 2016
Accepted article online 19 DEC 2016
Published online 12 JAN 2017

Abstract Since there are currently no magnetic field measurements made at Mars' surface, it is not possible to directly monitor the temporal variability of the external field as it is done on Earth's ground magnetic observatories. In this paper we examine two indirect ways of quantifying this external field. First, we directly use Mars Global Surveyor magnetic field measurements to quantify the level of variability of the external field. We sort the measurements on a fine spatial mesh, 0.8° × 0.8° at the equator. We then subtract for each bin and measurement the internal, crustal (static) field without any a priori modeling. We finally compute daily averages of the individual residuals to obtain a time series of an in situ proxy. Second, we use the Advanced Composition Explorer mission which measures the solar wind about 1 h upstream of the Earth at the L1 Lagrange point. These measurements are extrapolated to Mars' position taking into account the orbital configurations of the Mars-Earth system and the average velocity of particles carrying the interplanetary magnetic field to obtain a remote proxy time series. We compare these time series and demonstrate that they are complementary. When Mars and the Earth are close to the same Parker spiral arm, in situ and remote series have correlation coefficients close to 0.5. We show how these series, or proxies, can help to select magnetic field measurements on Mars. This dual approach and these proxies will especially be useful for upcoming magnetic field measurements made around or at the surface of Mars.

1. Introduction

Mars possesses no dynamic magnetic field of internal deep core origin as is the case for the Earth or for Mercury. Instead, Mars is characterized by an intense and localized magnetic field of crustal origin. This field is the result of past magnetization and demagnetization processes and reflects Mars' evolution of its interior and surface. Some parts of the planet, especially in the southern highlands, are associated with very intense magnetic fields, up to 1500 nT at 90 km altitude as was recorded by the magnetic field experiment on board MGS—Mars Global Surveyor [*Acuña et al.*, 1999]. More than half of the planet is devoid of significant crustal magnetic field at satellite altitude [*Langlais et al.*, 2004], which creates a heterogeneous picture of the Martian magnetic field.

This crustal internal magnetic field nonetheless interacts with Mars' ionized environment to create a complex external magnetic field system. Because it is closely related to the Sun, the external field displays a periodicity in relation with the position of the Sun and has also a signature which can be connected to the solar wind. The crustal field of Mars is very heterogeneous, and the interactions may therefore be diverse, depending both on the location and the local time [*Brain*, 2006]. This very dynamic external field may hamper the detailed modeling and analysis of the internal, crustal magnetic field at some places or times [*Jackson*, 2007; *Finlay et al.*, 2016].

The monitoring of the temporal and spatial variations of the external magnetic field is important for several aspects. First, the consequences of intense solar activity can damage Earth's-orbiting spacecraft's instruments or even reach the surface and cause major troubles to electrical network (see, for instance, descriptions and studies of a major solar storm in 2003, known as the 2003 Halloween magnetic superstorm [*Dryer et al.*, 2004; *Kappenman*, 2005, and references therein]). In the case of Mars, it is well known that energetic particles of the solar wind interact directly with the surface [*Crider et al.*, 2005]. Localized but intense magnetic field anomalies in the southern hemisphere may create mini-magnetospheres, and auroras were recorded in their vicinity [*Leblanc et al.*, 2008]. A second aspect is related to the properties of the Martian interior in relation with electromagnetic induction studies [*Civet and Tarits*, 2014]. It is possible to infer the electrical conductivity parameter through the separation of the time varying inducing external field and of the induced magnetic response by

conductive shell(s) inside the planet. Detailed characterization of the Martian crustal magnetic field anomalies and of their sources also depends on the quality of the measurements and on our ability to separate internal and external field variations. All these topics, therefore, require some knowledge and description of the external magnetic field temporal variability.

There are currently no magnetic field measurements made at Mars' surface, and it is not possible to directly monitor its temporal variations as it is done on Earth. We can, however, explore alternative ways to estimate this variability. In this study we examine two indirect ways to quantify and characterize this external field and to possibly improve the data selection for internal field studies. The first one is local, as it is based on in situ MGS magnetic field measurements. The second one is referred to as a remote approach, and it makes use of solar wind measurements around the Earth and extrapolated to Mars' position. These two approaches are complementary, as it is discussed in the following sections. These time series, or proxies, can be used a posteriori to analyze existing measurements, but the remote proxy can also be used in near real time, provided that Mars and the Earth are in favorable positions.

The outline of the paper is the following. After a description of some external field variations on Mars, we present two methods (in situ and remote) to derive time series characterizing the external field temporal variability on Mars. We then describe the results and discuss long-term, short-term, and spatial variations of the local time series and compare the in situ and remote results. We briefly discuss how our results may be used to define quiet versus active magnetic periods and to improve data selection for internal field studies. We finally conclude the paper by giving some possible future use and directions.

2. Observed External Magnetic Field Variability

Mars Global Surveyor stayed in orbit around Mars between September 1997 and November 2006. During the first 18 months MGS was on an elliptical orbit, until March 1999 when it started its Mapping Orbit cycles. The characteristics of the orbits were the following. MGS flew on a Sun-synchronous orbit, at 2 P.M. and 2 A.M. The altitude varied between 370 and 438 km, but the periapsis was fixed in latitude. MGS completed 100 mapping cycles, each cycle lasting 28 days, with a complete coverage of the planet every 88 orbits or 7 days. As a consequence, MGS visited each location (within 1°) at a constant altitude roughly once a week.

This particular geometry allows to focus on variable (external) versus static (internal) magnetic fields: every time the satellite flies above a given location, it senses the same internal magnetic field, and any observed variation between measurements acquired at different times may be related to external origin. This is illustrated by Figure 1, where we show seven orbits crossing the equator between 144.4 and 150.0° east longitude. Each orbit is separated by 7 days, as denoted by the day of year (DOY) value for year 2003. Only nightside measurements are shown, and there is no correction to remove any crustal field from an a priori model. There is a global trend which is reproduced for at least five orbits, with a field decreasing in intensity between −10 and 5° latitude, from about 30 to 5 nT, followed by a field increasing, up to about 15 nT. Two orbits present a different signature. On DOY 303 the field reaches about 45 nT slightly north of the equator, much more than what was measured 1 week before. On DOY 311, it does not increase in the northern hemisphere anymore but stays at a low level.

This feature was already observed by *Crider et al.* [2005] and reported as being associated with the occurrence on Mars of a huge coronal mass ejection which took place a couple of days earlier. It corresponds to the 2003 Halloween magnetic superstorm. The trajectory of the solar wind is usually approximated by an arithmetic spiral, known as the Parker spiral [*Parker*, 1958]. Whenever Mars and the Earth are close to the same arm of the Parker spiral (Figure 2 and subsection 3.2), the transit time between the Earth and Mars can be estimated. On 28 October 2003, and assuming a mean solar wind speed of 400 km s^{-1}, the total travel shift between the Earth and Mars would have been close to 3.8 days. We note, however, that for this particular event, the solar wind was much faster, as velocity measurement up to 2000 km s^{-1} was reported when it passed the Earth [*Skoug et al.*, 2004], implying a traveltime between the Sun and the Earth shorter than 1 day. *Crider et al.* [2005] reported an average speed close to 1340 km s^{-1} between the Sun and Mars for the same event. The traveltime from the Earth to Mars was under 1 day, thus implying an important slowdown after crossing Earth's orbit.

This example illustrates the high variability of the magnetic field around Mars related to the external activity. The magnetic field measured during active periods can be 3 times that measured during normal, quiet periods. The situation on the dayside (not shown) can be even worse. This motivates our study, which aims at

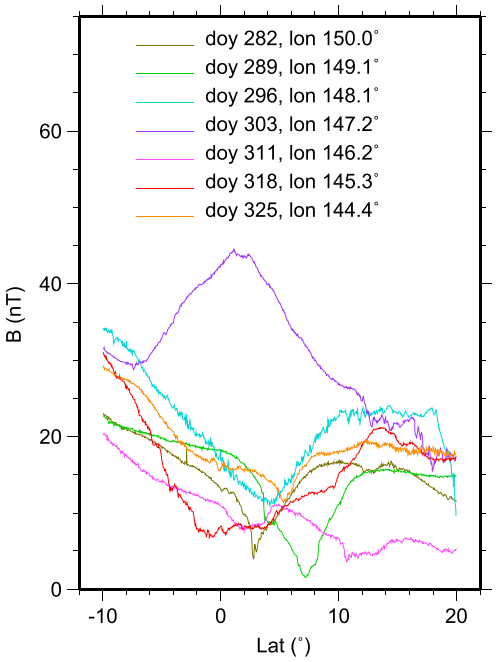

Figure 1. Total field measurements acquired during seven orbits between DOYs 282 and 325 of 2003 and passing over the same location.

characterizing the external field and its temporal variability on Mars on a global scale, in a similar way to what is done on Earth.

3. Method

3.1. In Situ Approach

Terrestrial external activity indices are based on ground observations. The magnetic field is continuously measured at several fixed locations. Daily periodic variations and transient ones can be straightforward identified and separated, and proxies for the external activity can be computed. There are no such observatories on

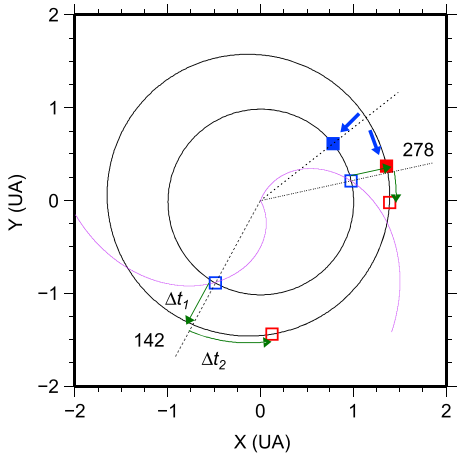

Figure 2. Mars' (red squares) and Earth's (blue squares) positions with respect to the Parker Spiral (in purple), at the beginning and end of period 3 as defined in the text (DOYs 142 and 278 of 2003, respectively). Δt_1 corresponds to the radial displacement (dotted line) from Earth's to Mars' orbit at the solar wind speed (assumed to be constant and equal to 400 km s^{-1}). Δt_2 corresponds to the along-orbit displacement, at the Sun's rotation speed ($\simeq$615 km s^{-1}). At the beginning of the period (label 142), $\Delta t_1 + \Delta t_2 \simeq 0$ (because $\Delta t_2 \leq 0$). At the end of the period $\Delta t_1 + \Delta t_2 \simeq 3.0$ days. Blue arrows and filled squares show the position of Mars and the Earth at the time of the 2003 Halloween magnetic superstorm (DOY 303).

Mars; as a consequence one must examine different ways to estimate such a proxy and to separate periodic from transient external magnetic field variations.

We follow a virtual observatory approach, in a similar manner to what can be done on Earth with spacecraft measurements *Mandea and Olsen* [2006]. We take advantage of the geometry of the MGS mission while it was in the Mapping Orbit phases. MGS flew over the same location and local time every 7 days or so. More than 50×10^6 measurements were acquired on each side (2:00 A.M. and 2:00 P.M.) and between $\pm 63°$ latitude. Polar areas are not considered in this study, because the local time changes too fast over these latitudes. Measurements are first sorted on an equisurface grid. A constant 0.8° latitudinal increment is considered, with a varying longitudinal one equal to $0.8 \times \cos(\text{latitude})$. The size of a bin at the equator is $0.8° \times 0.8° \simeq 2200\ \text{km}^2$. In the sorted data set, the observed altitude range does not vary by more than 5 km for all but a few bins and is always lower than 8 km. There are on average 878 measurements per bin, acquired during (on average) 74 different orbits or days. These numbers guarantee that the measured magnetic field time series over a specific location is representative of both the static magnetic field (both of crustal and external origin) and its temporal variations, if any.

In the following we use two coordinate systems. The first one is denoted MBF for Mars Body Fixed, a planeto-centered Cartesian system in which Z is along the rotation axis, X is perpendicular to Z and lies in the equatorial plane in the direction of the prime meridian as defined by the IAU, and Y completes the right-handed set. The second one is denoted MSS for Mars-Sun State reference frame. X always points toward the Sun, Z is northward perpendicular to the orbital plane, and Y again completes the right-handed set. In this second system, dayside corresponds to positive X.

We consider the three components of the measured Martian field in the MBF reference frame and on the nightside. For each equisurface bin the median magnetic field is identified. This median value at a given location may be seen as the static field for this location, regardless of its origin (internal or external). It is further independent of any a priori model which could be used to remove the crustal field. This median value is subtracted from individual measurements, and the individual residuals are then rotated to the MSS coordinate system. This leads to sparse time series of magnetic field components in the MSS system for each geographic bin. Finally, all individual residuals of all bins are considered to compute statistics on varying time windows and for the entire planet. We consider the Martian daily arithmetic mean, hereafter denoted L1N, and the associated Martian daily standard deviation, hereafter denoted L2N. The letter N is chosen because these quantities refer to the nightside measurements. Similar statistics are computed on the dayside, by subtracting from the measurements the median value estimated with the nightside measurements. These dayside quantities are denoted L1D and L2D, respectively (D for the dayside).

3.2. A Remote Approach

An alternative possibility to monitor the temporal variation of the external field at Mars is to consider measurements made close to the Earth and extrapolated to the position of Mars. For this purpose we use measurements made by the NASA mission Advanced Composition Explorer (ACE) launched in 1997. This mission monitors the characteristics of the solar wind and of the interplanetary magnetic field (IMF) at the L1 Lagrange point between the Earth and the Sun. At this location the satellite captures parameters of the solar wind about 1.5×10^6 km or 1 h upstream of the bow shock resulting from interaction of the solar and the Earth's main magnetic field (assuming a constant solar wind speed at 400 km s^{-1}). These measurements are thus solely sensitive to the solar wind temporal variability.

These measurements may be extrapolated to Mars' position [*Civet and Tarits*, 2014]. The IMF is propagated along Parker's spiral arms (see Figure 2), only when the Earth and Mars are close to the same arm. The time shift we compute takes into account both radial Δt_1 and along-orbit Δt_2 displacement. A constant solar wind speed of 400 km s^{-1} is assumed for Δt_1. This is a very simple assumption, as there were no measurements of the solar wind at Mars prior to Mars Atmosphere and Volatile EvolutioN (MAVEN) [*Halekas et al.*, 2015]. This assumption also allows to ignore the effects of stream interactions [*Vennerstrøm et al.*, 2003] which otherwise would have to be taken into account if using the measured solar wind velocity by ACE. At this mean speed, the solar wind takes about 1.6 days to travel from Earth's orbit to Mars' orbit (at perihelion). The difference in solar longitude between Earth and Mars is also taken into account by Δt_2 which assumes a Sun rotation period of 27 days [*Vennerstrøm et al.*, 2003; *Edberg et al.*, 2010]. This along-orbit correction may thus be negative and cancel out the radial one, if Mars is located ahead of the position of the Earth at its orbit.

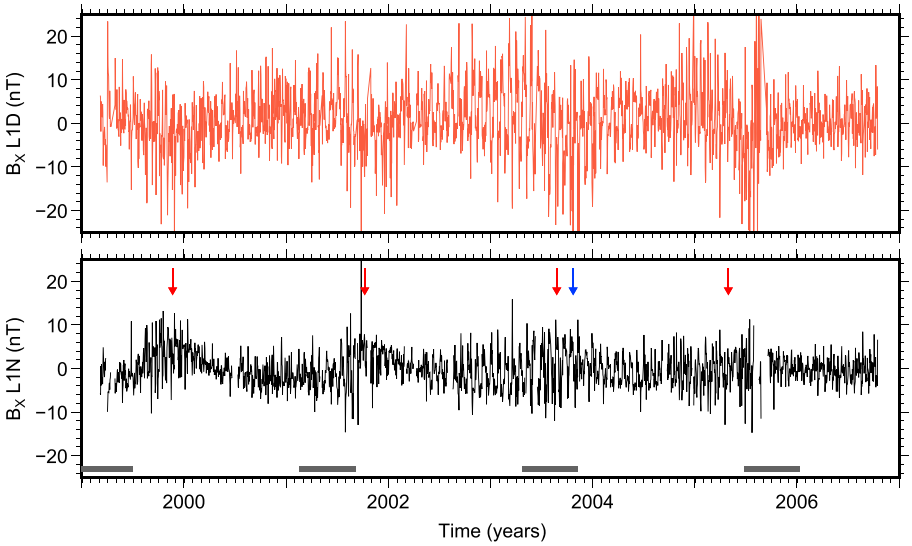

Figure 3. Daily magnetic (top) L1D and (bottom) L1N time series (B_X MSS component). Horizontal bars in Figure 3 (bottom) indicate the four periods when Mars and Earth were close to the same arm of the Parker spiral. Red arrows denote perihelion, and the blue arrow corresponds to the occurrence of the 2003 Halloween magnetic superstorm on Mars.

As for the in situ magnetic field approach, only the B_X component (with X pointing toward the Sun) is taken into account. The time-shifted, 1 Hz measurements are averaged on a Martian daily basis. The arithmetic mean and the standard deviations are computed and denoted L1R and L2R, respectively (R stands for remote). In the following we impose the total time shift to lie between 0 and 3 days, which restricts the time period to a duration of about 120 to 140 days. Computing the full time series since the beginning of the MGS mission is not possible, because ACE measurements cannot be continuously extrapolated to Mars' orbit.

4. Results

4.1. Long-Term Trends

The in situ and remote approaches allow the different quantities and time series to be compared and discussed. We first show in Figures 3 and 4 the in situ MSS B_X component L1 and L2 nightside and dayside time series, respectively. The entire time series goes from March 1999 until November 2006. The B_X component was chosen as this is the one showing the most variability on the nightside. The dayside series shows larger

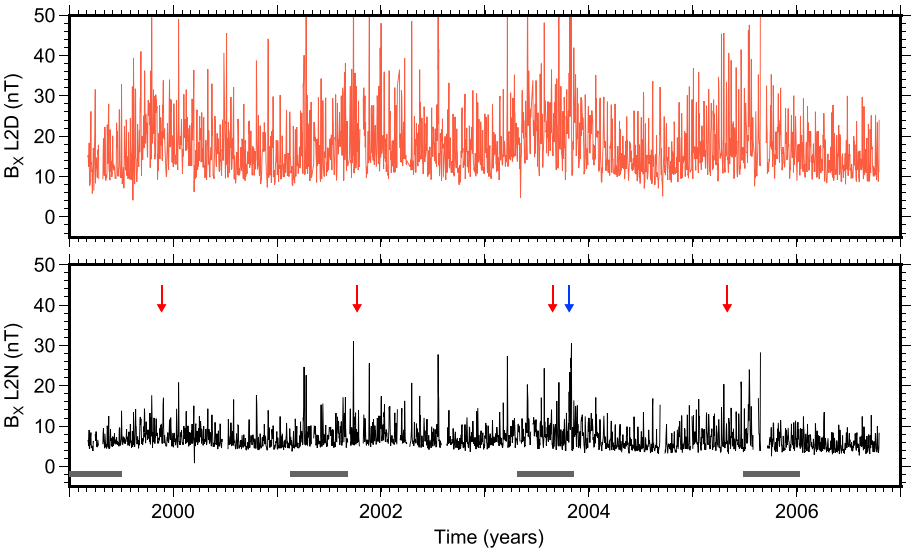

Figure 4. Same as Figure 3 but for the L2D and L2N time series.

amplitudes (±15 nT on average on the dayside versus ±7 nT on the nightside); this is related to the solar wind which directly interacts with the planetary atmosphere [*Brain et al.*, 2003]. The time series for the B_Y and B_Z components are given as supporting information, Figures S1 to S4. It should be noted that the B_Y component displays a strong variability on the dayside too, which is anticorrelated to the dayside B_X one. The amplitude of the nightside B_Y component is, however, very weak, generally remaining below ±1 nT, with extrema at ±4 nT. Similar observations can be done with the B_Z component. At MGS mapping altitude (400 km), the tail lobe is not flared.

First, looking at the L1 time series (Figure 3), one can see a clear and visible periodic component in L1D and L1N time series. Both series indeed display a long-term periodic variation, whose period is the rotation period of Mars around the Sun (687 days, close to 22 months). Such a periodicity was already observed [e.g., *Brain*, 2006]. B_X reaches a maximum (minimum) level on the nightside when Mars is at perihelion (aphelion). The correlation coefficient between the dayside and nightside time series is equal to −0.788 for the entire time interval. The B_Y component is anticorrelated with B_X on the dayside, with a correlation coefficient of −0.840. This is also consistent with draping patterns of the solar wind magnetic field around Mars [*Crider et al.*, 2004]. However, it shows only a weak annual periodicity on the nightside and is not correlated with the dayside one. The third component B_Z shows no clear trend and is not correlated to B_X and B_Y (correlation coefficients lower than 0.1).

The L2 time series aim at looking at the temporal variability of the signal. When this L2 quantity is at a low level, the external field is more stable over a given period. Maximum values inversely correspond to disturbed days. Looking at these L2D and L2N time series (Figure 4) reveals an almost annual cycle, which is especially visible on the dayside. The difference in amplitude of the signal is more important between both times series, 35 nT on the nightside versus 60 nT on the dayside. B_X has globally larger values when Mars is at perihelion. This is however not systematic, as, for instance, the peak seems to postdate the 2003 and 2005 perihelions. The lowest values are also lower on the nightside. On the nightside a global decreasing trend can be seen, with a mean L2N proxy which is 10% less intense in 2006 than in 1999. This may be related to the decreasing solar activity, with a solar minimum reached in 2008. Dayside and nightside proxies remain remarkably correlated, with an overall correlation coefficient equal to 0.856 for the entire period.

4.2. Short-Term Trends

It is necessary to reduce the considered time interval in order to investigate shorter-term trends and variations. There are 6 independent time series containing more than 200 consecutive L1 and L2 estimates. The longest one spans the time interval between 2003.46 and 2004.69 and contains 436 and 447 samples for the nightside and dayside time series, respectively. We show these time series in Figure 5.

During the considered time interval, the dayside and nightside series are anticorrelated at −0.820. The MSS B_X changes sign every 13 days on average, with a repeated pattern having a 26–27 day periodicity. This period corresponds to the rotation of the Sun. Such periodicities were already observed for the draping direction of the solar wind magnetic field [e.g., *Brain et al.*, 2006] but for a more limited time period and above northern latitudes only. On the dayside, the B_X and B_Y (not shown for the specific period, but it can be seen in the supporting information) have a correlation coefficient equal to −0.890, while there is no correlation between these components on the nightside.

We high-pass filtered the L1D and L1N time series for this time interval. We use a cosine-taper, rejecting all periods larger than 20 days and passing those smaller than 15 days. These filtered time series are shown in Figures 5b and 5c. The signal becomes very small on the nightside, lower than a few nT on average, although the correlation coefficient between the unfiltered and filtered time series remains at 0.672. On the dayside this coefficient is equal to 0.695, and the filtered L1D has ±10 nT extrema.

These extreme values in the L1 series are not reached when the Halloween magnetic superstorm hit Mars on 30 October 2003, i.e., DOY 305 of 2003. It is indicated with a blue arrow in Figure 5. There is no clear signature in the L1D and L1N series: the abrupt decrease could tentatively be seen as evidence of this event, but such decreases are seen at other time periods. In addition, the filtered times series show no special behavior around that day.

The L2D an L2N time series (Figures 5d and 5e) remain remarkably similar, with a correlation coefficient equal to 0.906. There is no 26–27 day periodic signal in those series, but there remains a 13 day one which is more visible in the L2D series. Because the L2 quantity is related to the stability of the external signal for a given day,

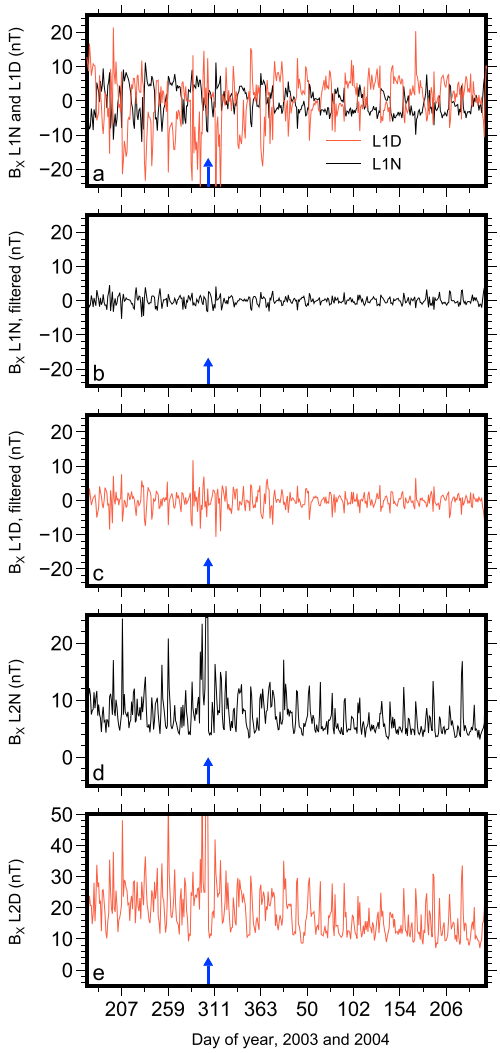

Figure 5. Comparison of the different time series between 2003.46 and 2004.69 (longest interval with consecutive time samples). (a) L1D (red) and L1N (black). (b) High-pass filtered L1N. (c) High-pass filtered L1D. (d) L2N. (e) L2D. On each panel the blue arrow corresponds to the occurrence of the 2003 Halloween magnetic superstorm on Mars.

this 13 day period simply corresponds to the sign change of the B_X component every 13 days. The dayside and nightside series have a mean value at 18.4 and 7.3 nT, but they may exceed 55 and 30 nT, respectively. These times series, especially the L2N one, can be used to identify magnetic events. There are, for instance, strong variations around the arrival of the Halloween magnetic superstorm. Around that day, L2D and L2N reach the second most intense values observed during the entire time series (the maximum was recorded during the second half of 2001). For comparison, on Earth this superstorm was associated with a *Dst* reaching a value as low as −400 nT, which is one of the most extreme values ever recorded.

4.3. Spatial Variations and Directions of the External Field

We have so far considered all the measurements, with the exception of those poleward of 63° absolute latitude. The crustal, static field is removed from each measurement, which allows a stacking on the dayside and the nightside. In this subsection we investigate possible latitudinal variations.

We follow the same approach as previously to compute north and south time series. We choose to retain measurements only between −40° and −30° latitude for the southern hemisphere, and between 30° and 40° latitude for the northern hemisphere. For consistency and clarity we restrict the time interval to the one between 2003.46 and 2004.69 (see the previous subsection). These time series are denoted L1Ds and L1Ns (L1Dn and L1Nn) for the southern (northern) hemisphere.

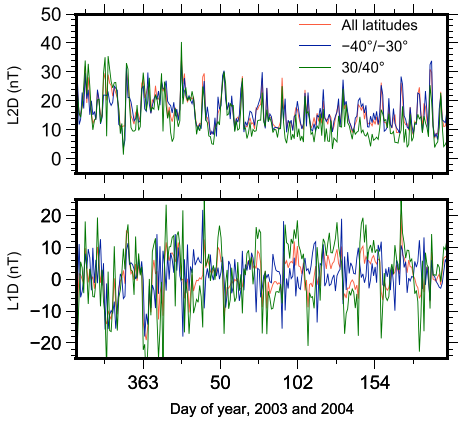

Figure 6. Comparison of the different L1D and L2D for all latitudes (red), −40°/−30° (blue) or 30°/40° (green).

The time series on the nightside are almost identical at northern and southern latitudes (correlation exceeds 0.840), but they slightly differ on the dayside, especially for southern latitudes. The correlation coefficient between that series and the L1D one decreases to 0.497, while it is 0.710 at northern latitudes. We show in Figure 6 the L1 and L2 time series on the dayside and for the northern, southern, or all latitudes. Note that the displayed time interval is shorter than for Figure 5, because the series has less consecutive estimates. The northern hemisphere series shows enhanced variations, with more positive or more negative values. On the contrary, the southern hemisphere series has less pronounced variations. Regarding the L2D series, the southern hemisphere series tends to show larger values, this is especially visible at the end of the displayed time interval. On the nightside, differences between the two hemispheres are not significant.

This north-south difference is further confirmed when looking at the mean orientation of the external field in the horizontal plane. We define $\alpha = \arctan(B_X, B_Y)$. For an external field pointing toward the Sun, $\alpha = 0°$. We show this angle in Figure 7, again for the time interval between 2003.46 and 2004.69. We binned the angles per 10°, and we present the results under the form of a rose diagram. The external field has two preferential directions on each side of the planet. On the dayside, it is mostly at −65°/115°, i.e., subperpendicular to the Mars-Sun direction. On the nightside it is mostly −15°/165°, i.e., at 50° of the dayside preferential directions and subparallel to the Mars-Sun direction. The same behavior is observed at northern latitudes (even if there seem to be a +10° shift with respect to all latitudes. The picture is very different for the southern latitudes, where the preferential directions remain similar but with less occurrence.

This spatial behavior of the external field around Mars is probably related to the dichotomy between the very intense magnetic field anomalies found in the southern hemisphere and their almost complete absence in the northern hemisphere. In the southern hemisphere the crustal field exceeds 100 nT in numerous locations at the altitude of the measurements. This crustal field interacts with the external field, creating so-called mini-magnetospheres [*Brain and Halekas*, 2013], and this may explain why the external field shows more diverse directions in the southern hemisphere.

4.4. Comparison With Remote Estimates

Finally, we compare our in situ estimates of the external field around Mars to the one we built by extrapolating ACE measurements to the location of the planet. This comparison is important for two reasons. First, the in situ approach can be validated by the remote one. Second, the remote approach can be used to monitor the external field variations at Mars even when there are no local measurements or when existing measurements are not suited for the in situ approach. There are four periods during which Mars and the Earth were close to the same arm of the Parker spiral, as indicated by the horizontal bars in Figures 3 and 4. In the following we focus on the second and third periods, in 2001 and 2003 (periods 1 and 4 occurred mid-1999 and at the end of 2005, respectively). It is important to note that Mars reached perihelion after period 2 and during period 3 (in August 2003).

We present these series in Figure 8. Because the in situ time series show much more variability than the remote one, a three-sample simple moving average filter is first applied to all series. The filtering is consistent with the maximum time shift of 3 days we impose. It also gives a lower limit on the expected temporal accuracy of

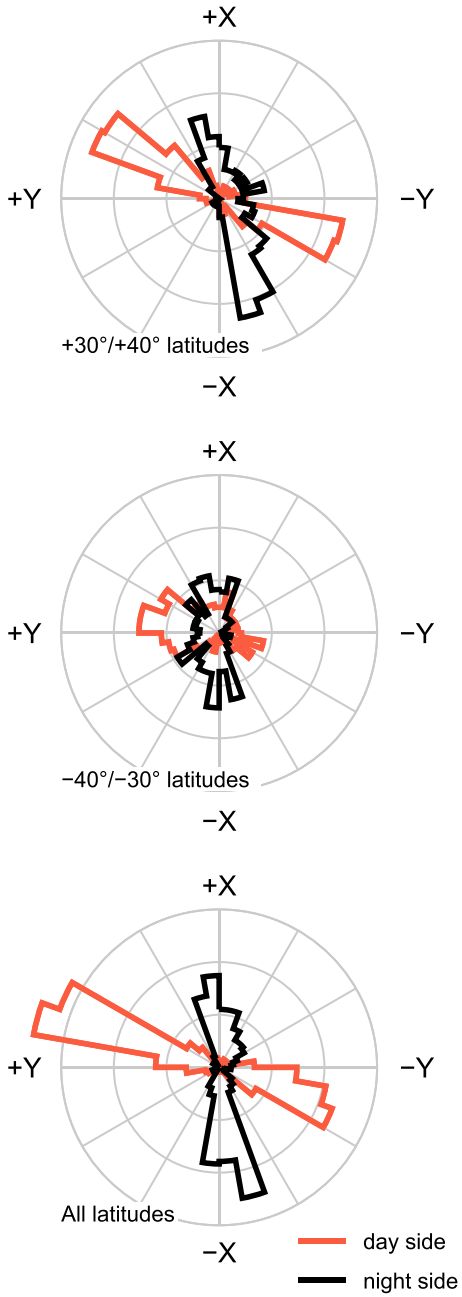

Figure 7. Angle distribution of the external field in the MSS *X*-*Y* plan (+*X* in the direction of the Sun), on the dayside (red) and nightside (black), and for different latitude ranges. Angle bins are 10° wide. The outer circle corresponds to 15%, and the intermediate ones to 5 and 10%, respectively.

the extrapolated remote proxy. A quick and visual comparison reveals that the in situ and remote L1 and L2 time series are anticorrelated and correlated, respectively. The L1R series is actually correlated with the L1D one, which is itself anticorrelated with the L1N one shown here (see Figure 5a).

As for the in situ time series there is a dominant period at 26–27 days in the L1R series. This is especially visible during period 3, when the series changes sign every 13 days or so. The amplitude of the signal is less important during period 2 and may blur the periodic signal. The L2R series shows very little periodicity, except maybe during period 3 where some sign changes in the L1R one are associated with slightly larger L2R values. That is however not a systematic feature, and this is not present during period 2. The amplitude of the signal is about half that of the local proxy.

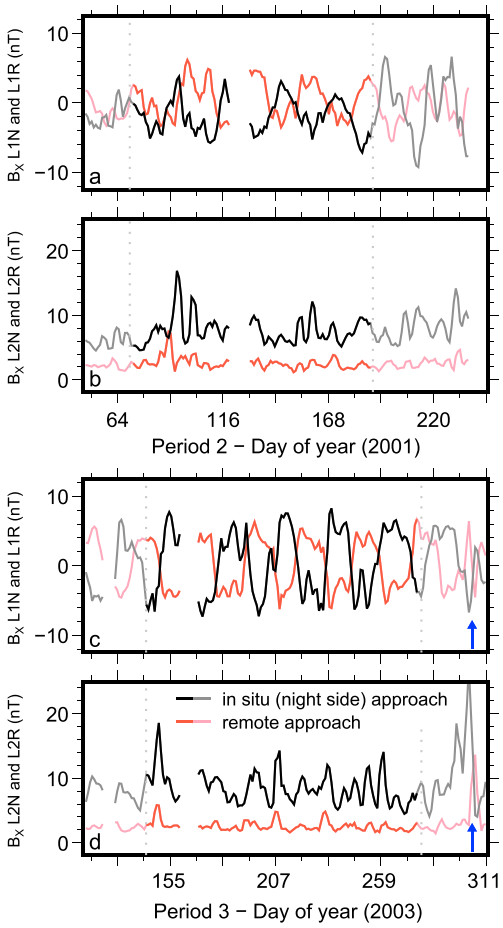

Figure 8. Comparison of the in situ nightside L1N and L2N (black) and remote (red) L1R and L2R time series. The time shift is between 0 and 3 days between the vertical dashed gray lines, and lower than 0 or larger than 3 outside them (gray and light red curves). (a) L1 and (b) L2 time series during period 2. (c) L1 and (d) L2 time series during period 3. Blue arrow corresponds to the occurrence of the 2003 Halloween magnetic superstorm on Mars.

The correlation coefficients between the different proxies are given in Table 1. They are of the order of −0.7 for the L1 proxies and close to about 0.5 of the L2 ones. The correlation is poorer for the first period, which is also the shortest one. The 2003 Halloween magnetic superstorm event is indicated in Figure 8 by the blue arrow. The magnetic field as measured by ACE reached only 68 nT, a large but not exceptional value [*Skoug et al.*, 2004]. There is a sharp decrease of the L1 proxy, while the L2 proxy abruptly increases from 3 nT to 16 nT. This signature is comparable to that observed with the in situ L1N and L2N series (Figure 5), although it seems

Table 1. Correlation Coefficients Between the Local L1N, L2N and Remote L1R, L2R Series for the Four Time Periods Considered in This Study[a]

	1.5 ± 1.5 (days)			1.5 ± 2.5 (days)		
Period	*N* (days)	L1	L2	*N* (days)	L1	L2
First	28	−0.674	0.166	60	−0.411	0.333
Second	106	−0.555	0.219	176	−0.434	0.247
Third	123	−0.836	0.665	180	−0.777	0.251
Fourth	67	−0.652	0.612	117	−0.462	0.435
All	324	−0.702	0.488	554	−0.555	0.304

[a]Left part corresponds to periods when the total time shift lies between 0 and 3 days, while the right part corresponds to periods when the total time shift is expanded to between −1 and 4 days. *N* is the number of days for the considered period.

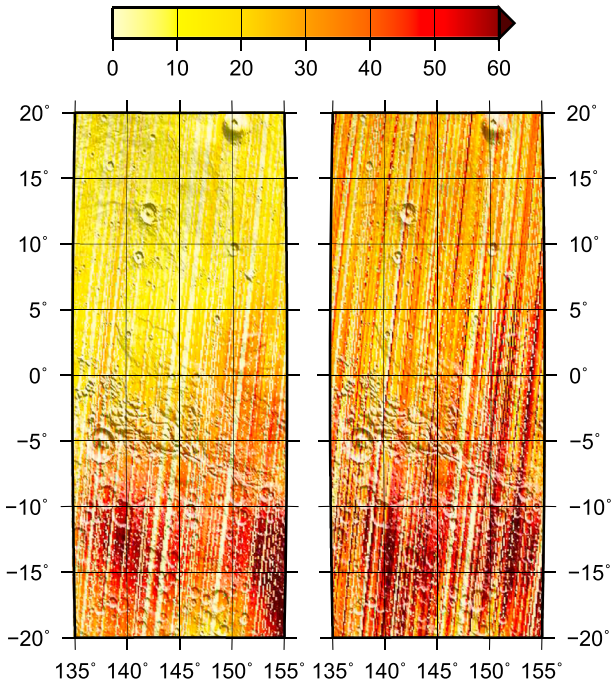

Figure 9. MGS total field measurements (nightside, about 400 km altitude) above the crustal dichotomy and south of Elysium Planitia. Remarkable features are Albor Tholus volcano (close to the north boundary) and craters Eddie (86 km, 12.3°N, 142.2°E), Gale (154 km, 5.4°S, 137.8°E), Wien (115 km, 10.6°S, 139.8°E), and Lasswitz (108 km, 9.3°S, 138.3°E). (left) Measurements acquired during the quietest days. (right) Measurements acquired during the most active days. Scale is in nanotesla.

to be shifted by 1 day or so with respect to the in situ approach. This event took place when the time delay (assuming a constant solar wind speed of 400 km s^{-1}) was slightly larger than 3 days, thus subject to larger errors and poorer temporal correlation. In addition, the solar wind was much faster, and this may explain why the remote proxy appears to be 1 or 2 days behind the local proxy.

When considering larger time intervals, corresponding to larger time shifts, the comparison between the in situ and the remote series becomes less favorable. They show more differences, with correlation coefficients decreasing to −0.5 and 0.3 for the L1 and L2 series, respectively. The extrapolation of solar wind magnetic field from the Earth to Mars is only possible during short, about 120 to 140 day long, time periods. In the absence of in situ measurements, the remote proxy may also have a poor time resolution, especially when strong events can be identified in the L2R time series. In this case the proxy may be late by 1 or 2 days. The proxy may still be used to select measurements, provided that the temporal behavior of the proxy is considered and not only its magnitude.

5. Discussion: Data Selection for Internal Field Studies

We now turn to a possible application of the in situ and remote approaches we develop to monitor the external field temporal variations. Indeed, such estimates on Earth are routinely used to select magnetic field measurements (at surface observatories or on board orbiting spacecraft) for internal magnetic field modeling purposes, in order to reduce the external magnetic field variability. So-called quiet/active periods are defined, corresponding to periods when the external field variability is low/large, using magnetic field proxies or activity indices. These are, for instance, the planetary index *Kp* or the ring current index *Dst*, which are routinely produced using ground observatory measurements [*Mayaud*, 1980]. In the end, only a small fraction (typically between 10 and 20%) of the available measurements are selected during these quiet periods and later used to derive geomagnetic field models [*Sabaka et al.*, 2015].

The L2N time series we present in the study is not sensitive to geographic location on Mars (similar behavior in the southern and northern hemispheres) and shows very little periodicity with the exception of moderate

peaks associated with sign changes in the L1N series. We therefore propose to use it as one would use the *Dst* or another external field proxy on Earth to identify quiet external field conditions and to select magnetic field measurements for internal field studies.

We present and compare in Figure 9 raw magnetic field measurements made during the quietest periods to those made during the most active ones, as defined by the in situ L2N time series or proxy. We define the quietest measurement days by limiting the L2N proxy to 4.5 nT. This corresponds to keeping 9.2% of the measurements. Conversely, the most active days are those during which the proxy is larger than 11 nT. It corresponds to keeping only 10.5% of the measurements. These maximum and minimum values are chosen so that they correspond to keeping about 10% of the measurements for the quiet and active times, respectively. It is interesting to note that most of the quietest days are found in the last 2 years of the mission, as is expected from Figure 4.

The differences between the two maps are striking. The quiet measurements allow the clear identification of magnetic highs and lows. The magnetic field is below 10 nT almost everywhere in the lowlands north of the dichotomy but on the eastern edge of the displayed area (this corresponds to Aeolis Dorsa). There are two magnetic highs, one slightly south of the Wien and Lasswitz craters, and another on the southeast corner. These two local highs cannot be distinguished on the disturbed right map, where the magnetic field above the lowlands is closer to 30 nT. Lithospheric field studies on the Earth have been shown to be very dependent on (drastic) data selection to eliminate transient external field and to improve the signal-to-noise ratio by keeping only the quietest time periods [e.g., *Thébault et al.*, 2016]. This problem has not been tackled on Mars yet because there were no such indices or proxies to identify these periods. This example highlights the possible use of the L2N proxy for data selection for crustal field modeling on Mars.

6. Conclusion

In this paper we describe nightside and dayside time series based on in situ measurements of the magnetic field around Mars to describe the external magnetic field variability. We use measurements which are repeatedly made at (or near to) the same location and correct these measurements from the ambient, static field, before computing daily averages and associated root-mean-square values. This is very similar to what is done for terrestrial indices, as they are computed from ground observatory magnetic field measurements. Our time series rely only on magnetic field measurements expressed in the Mars-Sun State reference frame, without any a priori modeling step. We make use of measurements acquired all around the planet, and we do not restrict our approach to areas where the crustal magnetic field is weak. The nightside (2:00 A.M.) and dayside (2:00 P.M.) daily mean horizontal (Sun pointing) magnetic field signals are extremely well anticorrelated, showing two main periods at 26-27 days and 22 months. The daily standard deviations on both sides of the planets do correlate and do not show any temporal periodicity. A closer look at the mean orientation of the external field on the dayside reveals that it is sensitive to the large magnetic field anomalies in the southern hemisphere. The external field is, however, well organized and is mostly almost perpendicular to the Sun-Mars direction on the dayside and almost parallel on the nightside.

We also consider magnetic field measurements made close to the Earth by ACE spacecraft and extrapolated to Mars. ACE continuously monitors the interplanetary magnetic field and the solar wind. The extrapolation assumes a constant solar wind speed radially between Earth's and Mars' orbit. When we limit the total time shift to lie between 0 and 3 days, we again observe a very good anticorrelation between the extrapolated L1R time series and the in situ L1N one, with the same period of 26–27 days and 22 months. The L2R and L2N proxies are also similar, with correlation coefficients close to 0.5.

The comparison of these nightside in situ (based on along-orbit measurements) and remote (extrapolated to Mars' orbit) time series confirms that magnetic events of external origin can affect the two planets. Our study further demonstrates that it is possible to use remote magnetic field measurements to monitor the external magnetic field activity on Mars, provided that Mars and the Earth are close to the same arm of the Parker spiral, and despite a poorer time resolution. This configuration occurs only during 120 to 140 day long time periods, i.e., 15% of the time. This is not the ideal case, but it may provide useful information in the absence of in situ measurements. At the same time, the in situ proxy, or more exactly its temporal difference with respect to the remote one, may provide some constraints on the propagation of strong interplanetary coronal mass ejection between the Earth and Mars [*Génot et al.*, 2010; *Falkenberg et al.*, 2011]. A geographical approach, in which areas of weak versus strong intense crustal fields would be separately considered, could also bring some

insights on the solar wind interaction with the Martian environment [*Brain et al.*, 2006]. Interesting features could also be identified when the MAVEN mission will return a complete local time coverage.

This nightside L2N time series will be used to improve the signal-to-noise ratio of the measurements used to model the internal magnetic field of Mars, using MGS and also MAVEN measurements. Because MAVEN has different orbital characteristics [*Jakosky et al.*, 2015], a slightly different approach will have to be considered, but the remote approach will still be used to validate the in situ one. This remote approach can also be used to study the electrical conductivity of Mars [*Civet and Tarits*, 2014; *Menvielle et al.*, 2000]. This indeed usually requires continuous time series of magnetic field measurements and some constraints on the geometry of the magnetic source, i.e., the external field. Our estimates can thus complete existing but incomplete local time series and describe the temporal variability of the external field, including its main direction. This will be especially useful during the forthcoming INterior Exploration using Seismic Investigations, Geodesy, and Heat Transport—InSight mission to Mars [*Banerdt et al.*, 2013]. This mission will deploy a Seismic Experiment for Interior Structure (SEIS) at the surface of Mars [*Lognonne et al.*, 2015]. This instrument is sensitive to magnetic field variations, and a magnetometer is included in the payload to monitor these variations. Our remote approach may be used to complete and validate these measurements, at least on the (Martian) daily timescale.

Acknowledgments
This work was supported by the Centre National des Etudes Spatiales in the context of the SEIS/InSight experiment. We are grateful to the Associate Editor and three anonymous reviewers for thorough and constructive reviews. The MGS MAG/ER data set was obtained from the Planetary Data System (PDS) at Planetary Plasma Interactions (PPI) node (http://ppi.pds.nasa.gov/). We thank the ACE Science Data Centre and the NSSDC (http://nssdc.gsfc.nasa.gov/space/).

References

Acuña, M. H., et al. (1999), Global distribution of crustal magnetization discovered by the Mars Global Surveyor MAG/ER experiment, *Science*, *284*, 790–793, doi:10.1126/science.284.5415.790.

Banerdt, W. B., et al. (2013), InSight: A discovery mission to explore the interior of Mars, in *44th Lunar and Planetary Institute Science Conference Abstracts, held March 18–22, 2013*, The Woodlands, Tex., LPI Contribution No. 1719, p. 1915.

Brain, D., and J. S. Halekas (2013), Aurora in Martian mini magnetospheres, in *Auroral Phenomenology and Magnetospheric Processes: Earth and Other Planets*, edited by A. Keiling et al., pp. 123–132, AGU, Washington, D. C., doi:10.1029/2011GM001201.

Brain, D. A. (2006), Mars Global Surveyor measurements of the Martian solar wind interaction, *Space Sci. Rev.*, *126*, 77–112, doi:10.1007/s11214-006-9122-x.

Brain, D. A., F. Bagenal, M. H. Acuña, and J. E. P. Connerney (2003), Martian magnetic morphology: Contributions from the solar wind and crust, *J. Geophys. Res.*, *108*, 1424, doi:10.1029/2002JA009482.

Brain, D. A., D. L. Mitchell, and J. S. Halekas (2006), The magnetic field draping direction at Mars from April 1999 through August 2004, *Icarus*, *182*, 464–473, doi:10.1016/j.icarus.2005.09.023.

Civet, F., and P. Tarits (2014), Electrical conductivity of the mantle of Mars from MGS magnetic observations, *Earth Planets Space*, *66*, 85, doi:10.1186/1880-5981-66-85.

Crider, D. H., D. A. Brain, M. H. Acuña, D. Vignes, C. Mazelle, and C. Bertucci (2004), Mars Global Surveyor observations of solar wind magnetic field draping around Mars, *Space Sci. Rev.*, *111*, 203–221, doi:10.1023/B:SPAC.0000032714.66124.4e.

Crider, D. H., J. Espley, D. A. Brain, D. L. Mitchell, J. E. P. Connerney, and M. H. Acuña (2005), Mars Global Surveyor observations of the Halloween 2003 solar superstorm's encounter with Mars, *J. Geophys. Res.*, *110*, A09S21, doi:10.1029/2004JA010881.

Dryer, M., Z. Smith, C. D. Fry, W. Sun, C. S. Deehr, and S. I. Akasofu (2004), Real-time shock arrival predictions during the Halloween 2003 epoch, *Space Weather*, *2*, S09001, doi:10.1029/2004SW000087.

Edberg, N. J. T., M. Lester, S. W. H. Cowley, D. A. Brain, M. Fränz, and S. Barabash (2010), Magnetosonic Mach number effect of the position of the bow shock at Mars in comparison to Venus, *J. Geophys. Res.*, *115*, A07203, doi:10.1029/2009JA014998.

Falkenberg, T. V., A. Taktakishvili, A. Pulkkinen, S. Vennerstrom, D. Odstrcil, D. Brain, G. Delory, and D. Mitchell (2011), Evaluating predictions of ICME arrival at Earth and Mars, *Space Weather*, *9*, S00E12, doi:10.1029/2011SW000682.

Finlay, C. C., V. Lesur, E. Thébault, F. Vervelidou, A. Morschhauser, and R. Shore (2016), Challenges handling magnetospheric and ionospheric signals in internal geomagnetic field modelling, *Space Sci. Rev.*, 1–33, doi:10.1007/s11214-016-0285-9.

Génot, V., et al. (2010), Space weather applications with CDPP/AMDA, *Adv. Space Res.*, *45*, 1145–1155, doi:10.1016/j.asr.2009.11.010.

Halekas, J. S., et al. (2015), MAVEN observations of solar wind hydrogen deposition in the atmosphere of Mars, *Geophys. Res. Lett.*, *42*, 8901–8909, doi:10.1002/2015GL064693.

Jackson, A. (2007), *Time-Dependent Models of the Geomagnetic Field*, Springer, pp. 948–953, Netherlands.

Jakosky, B. M., et al. (2015), The Mars Atmosphere and Volatile EvolutioN (MAVEN) mission, *Space Sci. Rev.*, *195*, 3–48, doi:10.1007/s11214-015-0139-x.

Kappenman, J. G. (2005), An overview of the impulsive geomagnetic field disturbances and power grid impacts associated with the violent Sun-Earth connection events of 29–31 October 2003 and a comparative evaluation with other contemporary storms, *Space Weather*, *3*, S08C01, doi:10.1029/2004SW000128.

Langlais, B., M. E. Purucker, and M. Mandea (2004), Crustal magnetic field of Mars, *J. Geophys. Res.*, *109*, E02008, doi:10.1029/2003JE002048.

Leblanc, F., et al. (2008), Observations of aurorae by SPICAM ultraviolet spectrograph on board Mars Express: Simultaneous ASPERA-3 and MARSIS measurements, *J. Geophys. Res.*, *113*, A08311, doi:10.1029/2008JA013033.

Lognonne, P., et al. (2015), Science goals of SEIS, the InSight seismometer package, in *46th Lunar and Planetary Institute Science Conference Abstracts, held March 16–20, 2015*, The Woodlands, Tex., LPI Contribution 1832, p. 2272.

Mandea, M., and N. Olsen (2006), A new approach to directly determine the secular variation from magnetic satellite observations, *Geophys. Res. Lett.*, *33*, L15306, doi:10.1029/2006GL026616.

Mayaud, P. N. (1980), *Derivation, Meaning and Use of Geomagnetic Indices, AGU Geophys. Monogr., 22*, AGU Geophys. Monographs; no. 22, Washington, D. C.

Menvielle, M., et al. (2000), Contribution of magnetic measurements onboard NetLander to Mars exploration, *Planet. Space Sci.*, *48*, 1231–1247.

Parker, E. N. (1958), Dynamics of the interplanetary gas and magnetic fields, *Astrophys. J.*, *128*, 664, doi:10.1086/146579.

Sabaka, T. J., N. Olsen, R. H. Tyler, and A. Kuvshinov (2015), CM5, a pre-Swarm comprehensive geomagnetic field model derived from over 12 yr of CHAMP, Ørsted, SAC-C and observatory data, *Geophys. J. Int.*, *200*, 1596–1626, doi:10.1093/gji/ggu493.

Skoug, R. M., J. T. Gosling, J. T. Steinberg, D. J. McComas, C. W. Smith, N. F. Ness, Q. Hu, and L. F. Burlaga (2004), Extremely high speed solar wind: 29-30 October 2003, *J. Geophys. Res.*, *109*, A09102, doi:10.1029/2004JA010494.

Thébault, E., V. Lesur, K. Kauristie, and R. Shore (2016), Magnetic field data correction in space for modelling the lithospheric magnetic field, *Space Sci. Rev.*, doi:10.1007/s11214-016-0309-5.

Vennerstrøm, S., N. Olsen, M. E. Purucker, M. H. Acuña, and J. C. Cain (2003), The magnetic field in the pile-up region at Mars, and its variation with the solar wind, *Geophys. Res. Lett.*, *30*, 1369, doi:10.1029/2003GL016883.